Earth and Planetary Science Letters 579 (2022) 117337

Contents lists available at ScienceDirect

Earth and Planetary Science Letters

www.elsevier.com/locate/epsl

Boron concentrations and isotopic compositions in methane-derived authigenic carbonates: Constraints and limitations in reconstructing formation conditions

Wei-Li Hong [a,b,c,d,*], Aivo Lepland [a,b,e], Kalle Kirsimäe [e], Antoine Crémière [f], James W.B. Rae [g]

[a] Geological Survey of Norway (NGU), Trondheim, Norway
[b] Centre for Arctic Gas Hydrate, Environment and Climate (CAGE), the Arctic University of Tromsø, UiT, Norway
[c] Department of Geological Sciences, Stockholm University, Stockholm, Sweden
[d] Baltic Sea Centre, Stockholm University, Stockholm, Sweden
[e] Department of Geology, University of Tartu, 50411 Tartu, Estonia
[f] Division of Geological and Planetary Sciences, California Institute of Technology, Pasadena, CA, United States of America
[g] School of Earth & Environmental Sciences, University of St Andrews, St Andrews, UK

ARTICLE INFO

Article history:
Received 3 February 2021
Received in revised form 17 November 2021
Accepted 5 December 2021
Available online 23 December 2021
Editor: L. Coogan

Keywords:
boron
methane-derived authigenic carbonate
transport-reaction modelling
early diagenesis

ABSTRACT

The boron content and isotopic composition ($\delta^{11}B$), of marine carbonates have the potential to constrain CO_2 chemistry during carbonate growth conditions. However, obtaining and interpreting boron compositions from authigenic carbonates in geological archives present several challenges that may substantially limit their application. In particular, contamination from non-carbonate phases during sample preparation must be carefully avoided, and a variety of controls on boron composition during authigenic growth conditions must be evaluated. To advance understanding of the use and limitations of boron in authigenic carbonates, we present data and modelling results on methane-derived authigenic carbonate (MDAC), a by-product of microbially mediated anaerobic oxidation of methane, taken from three cold seep sites along the Norwegian margin. We present a novel sequential leaching method to isolate the boron signals from the micritic (Mg-calcite) and cavity-filling (aragonitic) MDAC cements in these complex multi-phase samples. This method successfully minimizes contamination from non-carbonate phases. To investigate the factors that could potentially contribute to the observed boron signals, we construct a numerical model to simulate the evolution of MDAC $\delta^{11}B$ and B/Ca ratios over its growth history. We show that diagenetic fluid composition, depths of precipitation, the physical properties of sediments (such as porosity), and mineral surface kinetics all contribute to the observed boron compositions in the different carbonate cements. While broad constraints may be placed on fluid composition, the multiple competing controls on boron in these diagenetic settings limit the ability to place unique solutions on fluid CO_2 chemistry using boron in these authigenic carbonates.

1. Introduction

Cold seeps are common seafloor features along both passive and active continental margins (Suess, 2014). The seepage and consumption of methane through anaerobic and aerobic microbial activities make cold seeps oases for life in nutrient-limited pelagic environments (Boetius et al., 2000). Precipitation of authigenic minerals in cold seeps, such as carbonates and sulphides, has also been suggested to influence the global carbon and sulphur cycles (Reeburgh, 2007). Methane-derived authigenic carbonates (MDACs) are commonly found from cold seeps (Loyd et al., 2016; Crémière et al., 2016b; Thiagarajan et al., 2020) where intensive anaerobic oxidation of methane (AOM) (Boetius et al., 2000) increases alkalinity (Eq. (1)) and stimulates carbonate precipitation with seawater calcium (Eq. (2); Luff and Wallmann, 2003):

$$\text{AOM}: CH_4 + SO_4^{2-} \rightarrow HCO_3^- + HS^- + H_2O \quad (1)$$

$$\text{Carbonate precipitation}: HCO_3^- + Ca^{2+} \rightarrow CaCO_3 + H^+ \quad (2)$$

* Corresponding author.
E-mail address: wei-li.hong@geo.su.se (W.-L. Hong).

https://doi.org/10.1016/j.epsl.2021.117337

Table 1
Mineral composition of the MDAC samples from Barents Sea, North Sea and Vestnesa Ridge.

sample #	Lab code	XRD-Carbonate (%)			XRD-Detrital (%)				
		Arg	Cal	Dol	Qz	K-Fsp	Pl	Mca	Chl
13C-1F	MC-M5	42.8	7.9	**BD**	38.5	7.1	2.2	1.4	**BD**
13C-1F	MC-M4	43.1	3.2	4.9	38.4	4.2	4.3	1.9	**BD**
21616-1-4CC	CFC-4CC-A	78.3	14.0	**BD**	3.5	1.2	**BD**	2.9	**BD**
21616-1-4CC	MC-4CC-M	73.1	6.1	**BD**	12.4	1.2	1.2	5.9	**tr.**
21637-1-12R	CFC-12R-A	86.7	7.2	**BD**	3.0	1.6	**BD**	1.1	**BD**
21637-1-12R	MC-12R-M	75.1	5.7	**BD**	9.2	2.2	1.2	6.7	**BD**
P1606-23C	23C-M	**BD**	**BD**	**BD**	93.7	1.6	**BD**	0.8	3.7

BD: below detection limit; tr.: trace amount; Arg: aragonite; Cal: Mg-calcite; Dol: dolomite; Qz: quartz; K-Fsp: K-feldspar; Pl: plagioclase; Mca: mica; Chl: chlorite.

The mixing between well-buffered basic fluids (pH >8), as a result of AOM, and less basic bottom seawater (pH ≈7.5), that contains low concentrations of dissolved inorganic carbon (DIC) and high concentrations of dissolved calcium, results in abrupt changes in carbonate saturation across the sediment-water interface, leading to the formation of MDACs (e.g., Reimers et al., 1996). The MDACs thus have the potential to record changes in fluid composition. MDAC formation is also thought to be a function of AOM rates, with fast carbonate precipitation occurring at shallow sediment depths when methane is rapidly consumed by AOM (Luff and Wallmann, 2003).

The different occurrences of MDACs, such as micritic and botryoidal cavity filling cements (MCs and CFCs, respectively; Figs. 1b-e), are thought to reflect different phases of carbonate precipitation and thus methane supply near the sediment-water interface (Peckmann et al., 2001; Himmler et al., 2010; Crémière et al., 2016b). The MCs precipitate during periods of lower methane supply, cementing existing detrital and/or biological sediment particles as templates and filling up the sediment pore space (Crémière et al., 2016b). The CFCs, which are mostly aragonite, occupy mm- to cm-size voids that have formed between MC-lithified sediment clasts. These voids are cracks that filled by endolithic biofilm colonies that are responsible for the formation of CFCs during periods of high seepage and thus high methane flux (Crémière et al., 2016b). Comparatively, the CFCs show rare earth element patterns influenced more by seawater suggesting precipitation closer to the bottom seawater (Crémière et al., 2016b; Schier et al., 2021). MDACs are frequently used to reconstruct the timing of seepage and fluid compositions along continental margins assuming that the precipitates are in equilibrium with the ambient fluids (Himmler et al., 2010; Crémière et al., 2016a). Recent studies, however, suggest apparent disequilibrium between MDACs and the ambient fluids for some geochemical proxies such as the carbonate clumped isotopic signature (Thiagarajan et al., 2020) and thus raise questions about reliable interpretation of geochemical proxies from MDACs. New methods of reconstructing conditions during MDAC formation are therefore valuable.

The boron isotopic signature ($\delta^{11}B$) and B/Ca ratio of biological carbonates have been used to reconstruct carbonate system conditions of the ocean (Vengosh et al., 1991; Hemming and Hanson, 1992; Foster, 2008; Rae et al., 2011; Hönisch et al., 2019) due to their dependency on pH and carbonate ion concentration (Mavromatis et al., 2015; Uchikawa et al., 2015). The proportion and $\delta^{11}B$ of the two dissolved boron species, boric acid and borate, is a function of solution pH (Dickson, 1990) (Fig. S1a) with a fractionation factor (α) of 1.0272 (Klochko et al., 2006) (Fig. S1b). During carbonate authigenesis, solution pH and $\delta^{11}B$ composition determine how much dissolved boron (mostly borate) and what $\delta^{11}B$ signatures will be incorporated (Hemming et al., 1995; Noireaux et al., 2015). As aragonite cements are the most common carbonate phase in our MDAC samples (Table 1), we will focus on the boron systematics of aragonite hereafter.

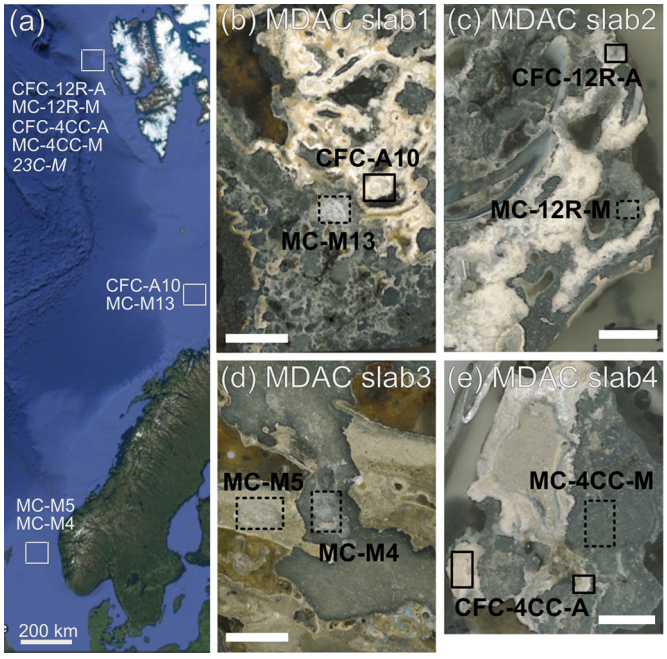

Fig. 1. (a) A map showing the locations of the seep sites investigated. CFC and MC stand for cavity-filling cement and micritic cement, respectively. Sample 23C-M is a consolidated siliciclastic sediment sample from Vestnesa Ridge. (b)-(e) Photos showing the locations where the micro-drilled samples were obtained from each of the four MDAC slabs. Dotted squares mark the sampling locations for MCs while the solid squares mark those for the CFCs. The carbonate cements, though appearing at adjacent locations, are not necessary formed under the same fluid seepage episode. The white bars are one centimetre. (For interpretation of the colours in the figure(s), the reader is referred to the web version of this article.)

Recent laboratory experiments on aragonite precipitation provide insights into the mechanism of boron incorporation (Noireaux et al., 2015) and how one can use boron proxies from corals (biogenic aragonite) to infer fluid chemistry during precipitation (Gagnon et al., 2021) and past pH (Rae et al., 2018). The B/Ca ratios in experimentally synthesized aragonites are sensitive to the concentrations of dissolved carbonate and borate, a relationship that can be expressed by partition coefficients (K_D) (DeCarlo et al., 2018). By considering published data on aragonite synthesis and solution composition, DeCarlo et al. (2018) proposed the following expression for K_D:

$$K_D^{B/Ca} = \frac{[B/Ca]^{aragonite}}{[B(OH)_4^-/CO_3^{2-}]^{solution}} = 0.00077 \cdot \mathrm{Ln}\left(\left[CO_3^{2-}\right]\right) - 0.0028 \quad (3)$$

where $[B/Ca]^{aragonite}$ and $[B(OH)_4^-/CO_3^{2-}]^{solution}$ are the molar ratios in aragonite and solution, respectively. The K_D of boron in aragonite appears to be independent from carbonate precipitation

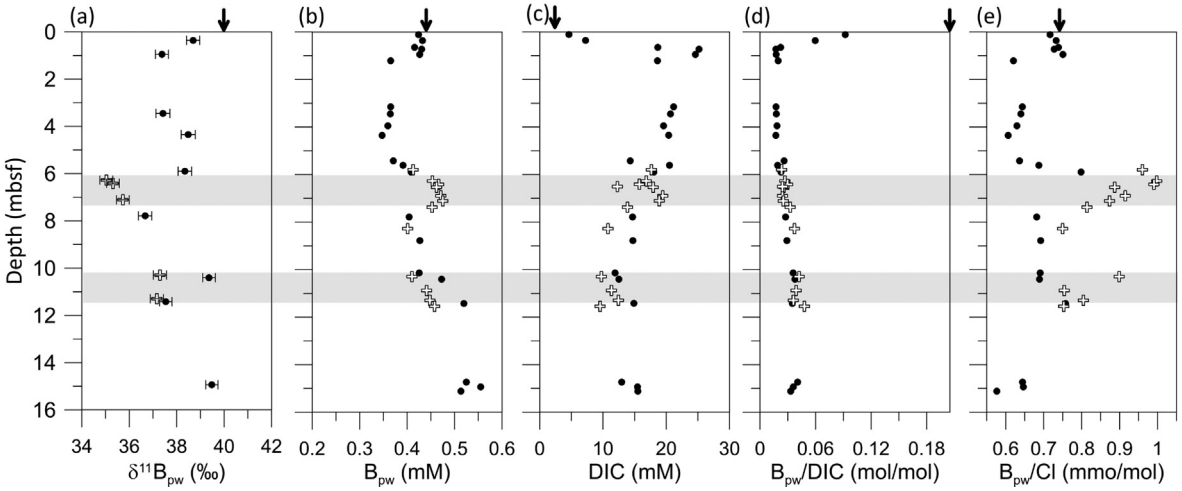

Fig. 2. Pore fluid boron composition (*a* and *b*) and B_{pw}/DIC ratios (*d*) from Vestnesa Ridge where four MDACs samples were collected. The arrows on the upper x-axes of all panels represent seawater composition. Empty crosses represent the samples influenced by gas hydrates that were recovered from the depths indicated by the grey shaded areas (Hong et al., 2021). MDAC samples investigated were recovered from the same two horizons containing gas hydrates. Anomalously low $\delta^{11}B_{pw}$ values indicate different B_{pw} sources while the concomitant increases in B_{pw}/Cl ratios (*e*) exclude gas hydrate dynamics as the cause for the high B_{pw} concentrations. The B_{pw}/DIC ratios show a sharp decline in the top 1 m with limited variation in greater depths, which reflect mostly the changes in DIC concentrations (*c*).

rates, a conclusion that can be arrived by examining the laboratory experiment data from Holcomb et al. (2016) (and in Fig. S3). As for the $\delta^{11}B$ of aragonite, it is predominately a function of pH (along with solution $\delta^{11}B$) with insignificant kinetic influence (Noireaux et al., 2015). In other words, the isotopic fractionation factor is not rate-dependent, a conclusion supported by the overlapping $\delta^{11}B$ values of the synthesized aragonite and $B(OH)_4^-$ in the solution (Hemming et al., 1995; Noireaux et al., 2015).

Though significant progress has been made in understanding the boron signatures from biogenic carbonate, obtaining and interpreting the $\delta^{11}B$ values and B/Ca ratios from the carbonate in rock or sediment presents a few major challenges. First and foremost, isolating the boron signatures of carbonates from samples with mixed mineral composition is challenging. A single-step chemical dissolution, as established for pure biogenic carbonates, may result in contamination by silicates, obscuring the carbonate signature for more mixed carbonate-silicate lithologies. Even if the carbonate signals can be successfully segregated, interpretation of the results is not straightforward. Unlike seawater, the composition of pore fluids in diagenetic environments of unconsolidated marine sediments (hereafter referred to as diagenetic fluids) could change dramatically within small time and space intervals. For example, in just a few meters below the seafloor, $\delta^{11}B$ values in pore fluids can vary by several permil (Fig. 2a) due to the mixing between seawater (+39.6 ‰; Foster et al., 2010) and fluids with lower $\delta^{11}B$ values from greater depths. Similarly, just one meter below the seafloor, the B/DIC ratios in pore fluids, which determine the B/Ca ratios in carbonates (cf. Eq. (3)), could be an order of magnitude lower than the seawater ratio (*ca*. 0.225 mol/mol; Fig. 2d). Besides the spatial variation, fluid composition also changes substantially with time as a result of biogeochemical reactions and/or environmental changes (Luff and Wallmann, 2003). It is thus challenging to comprehensively consider all spatial and temporal changes in fluid composition that affect the boron signals in authigenic carbonates. In addition, some critical parameters, such as fluid pH, are often not available due to the difficulties in obtaining in-situ values. These challenges limit the applicability of boron from impure carbonates forming in the diagenetic realm, though the few available studies (e.g., Deyhle and Kopf, 2001) have highlighted the potential insights if these limitations can be dealt with.

To overcome the hurdle of contaminations from non-carbonate phases, we develop a sequential leaching protocol to obtain representative boron signals from MDAC samples. To investigate factors that affect the $\delta^{11}B$ and B/Ca from MDAC, we construct a transport-reaction model calibrated with literature data for aragonite formation. We explore plausible ranges of fluid composition that explain the boron signals obtained from MDACs and identify factors that may be equally important when interpreting the results. We show that changes in pore water composition linked with biogeochemical reactions and fluid mixing contribute primarily to the observed changes in boron signatures from MDACs. Additional factors, such as the depths of carbonate precipitation, changes in sediment physical properties and even mineral surface kinetics, all play important roles in determining the boron signals in carbonates from rock and sediment records. The complex interaction of these factors may limit how much one is able to constrain past conditions based on the observations of boron systematics from geological carbonate archives.

2. Materials and methods

We report data from five micritic cements (MCs) and three cavity-filling cements (CFCs) occurring adjacent to each other in four MDAC crust slabs (Figs. 1b-e, Tables 1&2) as well as one consolidated siliciclastic sediment from one of the slabs (sample 23C-M in Tables 1&2). The MDAC crusts were collected from three locations: Alvheim channel in the central North Sea, Loppa High area in the south-western Barents Sea, and Vestnesa Ridge, west of Svalbard (Fig. 1a). Alvheim (samples MC-M4 and MC-M5) and Loppa High (samples CFC-A10 and MC-M13) MDAC crusts were collected from the seafloor by remotely operated vehicles (Crémière et al., 2016b). Vestnesa Ridge MDAC crusts (samples CFC-4CC-A, MC-4CC-M, CFC-12R-A, and MC-12R-M) and the siliciclastic sediment sample (23C-M) were collected during the cruise MSM57-1/2 onboard 'RV MARIA S. MERIAN' (Bohrmann et al., 2017) with the seafloor drill rig MARUM-MeBo70 (Freudenthal and Wefer, 2013). They were recovered from depths *ca*. 10 and 16 mbsf (Himmler et al., 2019) at a location within the active Lunde pockmark at the Vestnesa Ridge (sites GeoB21637-1 and GeoB21621-1). The Vestnesa Ridge samples we analysed have ages ranging from 42 to 156 ka (Himmler et al., 2019). Pore fluid data from the same location were also reported (Fig. 2) and described in detail by Hong et al. (2021).

Table 2
$\delta^{11}B$ and elemental ratios of the investigated MDACs.

MDACspl	Area	Ca **mM**	Al μ **M**	B/Ca **µmol/mol**	Mg/Ca **mmol/mol**	Al/Ca **µmol/mol**	$\delta^{11}B_{MDAC}$ ‰	f_{Si} ± **%**	corr-$\delta^{11}B_{MDAC}$ ‰	corr-B/Ca **µmol/mol**
CFC-A10	BS	50.4	2.5	72.0	1.3	49.4	13.5	0.3	13.5	71.8
MC-M13	BS	26.4	19	50.6	1.9	731.6	12.3	5.4	13.1	47.9
MC-M5	NS	30.2	3.3	47.2	32.6	112.6	12.4	1.0	12.6	46.8
MC-M4	NS	22.5	0.1	30.9	9.5	8.5	10.3	0.1	10.3	30.8
CFC-4CC-A	VR	46.2	1.1	23.1	0.7	24.0	12.6	0.4	12.6	23.0
MC-4CC-M	VR	95.0	34	64.2	4.8	361.8	6.9	2.1	7.1	62.8
CFC-12R-A	VR	46.5	0.1	29.4	0.9	2.9	13.0	<0.01	13.0	29.4
MC-12R-M	VR	95.4	0.5	20.4	4.6	4.6	9.9	0.1	9.9	22.0
23C-M	VR	0.1	122	3951.2	50.1	1.04E6	−2.0			

± We used $\delta^{11}B$ (−2.0 ‰) and B/Al (3775.5 µmole/mole) values from 23C-M to calculate the B contribution from silicate phases. See *Supplementary material* for the exemplary calculation for sample MC-M13. BS: Barents Sea; NS: North Sea; VR: Vestnesa Ridge.

2.1. Extraction and analysis of boron signals from MDACs

The sequential leaching protocol applied to the eight MDAC samples and one background sediment sample consists of three treatments: (i) an oxidative cleaning step (3 vol% H_2O_2 with occasional hot water bath) to remove organic material, (ii) a buffered solution (0.5 M NH_4Ac) to remove the adsorbed exchangeable ions, and (iii) a final 10-step acid leaching with 0.25 to 10 vol% HAc. An aliquot of the leachate was analysed for minor and trace elements with an Agilent 7500 ICP-MS following previously published protocols (Rae et al., 2011; Shao et al., 2019). Depending on the concentration of boron in the samples, 500 to 1000 µl of the leachate was put through the boron-specific anionic exchange resin Amberlite IRA 743 (Kiss, 1988) to isolate 2-10 ng of boron largely following the procedure of Foster (2008). The pH in diluted HAc leachate was between five and six so these samples require no additional pH adjustment before loading onto columns. For concentrated HAc leachate, samples were mixed with equal volumes of NH_4Ac buffer to adjust pH to values higher than five before the column separation. Boron isotopes were analysed with a Thermo Finnigan Neptune Plus MC-ICP-MS, following Foster (2008) and Rae et al. (2018), with the use of 0.3 M HF to improve boron washout from the spray chamber, as discussed by Zeebe and Rae (2020). Boric acid consistency standards, AE121 and BIGD (Foster et al., 2013), were run with every batch as a check on accuracy and instrument precision. Long-term reproducibility during this analytical campaign on samples of this size was 0.15 ‰ (2SD, $n = 20$).

Guided by the trace element composition of the leachate, we consider the extractions with moderately diluted HAc (0.5 to 1 %) as being the most compositionally representative of carbonate. The $\delta^{11}B$ values and B/Ca ratios for the eight MDAC were further calibrated based on the aluminium concentrations in the leachate (0.1 to 34 μ M; Table 2), which can trace silicate contamination. Such aluminium concentrations are comparable to those obtained by Bellefroid et al. (2018) using sequential leaching and two to three orders of magnitude lower than single-step leaching with nitric acid (e.g., Paris et al., 2010). Nonetheless, the trace amounts of aluminium indicate minor contributions from silicate minerals. We therefore corrected the data with the results obtained from the siliciclastic sediment sample from Vestnesa Ridge (23C-M in Table 2) assuming a binary mixing between the MDAC and silicate associated boron. More details about how the correction is done can be found from the *Supplementary Material*.

2.2. Pore fluid analyses

Dissolved boron concentrations were determined by inductively coupled plasma atomic emission spectroscopy (ICP-AES). Concentrations of DIC were approximated by subtracting the shipboard-titrated total alkalinity (TA) with the concentrations of total dissolved sulphide (ΣHS) (see methods described by Hong et al., 2020). The dissolved boron was isolated and analysed for $\delta^{11}B$ following the same protocols described in section 2.1 for MDAC samples. Pore fluid sulphate concentrations, measured by ion chromatography, have been previously reported in Pape et al. (2020). The B in the porewater is referred as B_{pw} (total dissolved B, including boric acid and borate) and the B in carbonate as B_{MDAC} or B_{arg} (boron in methane-derived authigenic carbonate or aragonite).

2.3. X-ray diffraction (XRD) method

About 10-30 mg of samples were pulverized by hand with an agate pestle and mortar under ethanol and preparations were made by dropping sample suspension on low-background silicon wafers. Dried preparations were scanned on a Bruker D8 Advance using CuKα radiation and LynxEye positive sensitive detector in 2–70° 2Θ range with step size 0.012° and counting time one second per step. The semi-quantitative mineralogical composition of the samples was interpreted and modelled using the Rietveld algorithm-based code Topaz by Bruker. Due to small sample size the relative error of quantification is *ca*. 20 %.

2.4. Numerical model configuration and calibration

We established a numerical model using the software routine CrunchFlow (Steefel et al., 2015) to simulate the incorporation of boron in aragonite in these environments. There are three primary components in this model: aqueous chemistry, the kinetic and thermodynamic parameterization of carbonate precipitation, and the kinetics of boron incorporation. These components are detailed in the *Supplementary material*. We simulated a small sediment column of 5-cm, a dimension that roughly corresponds to the size of our MDAC slabs (Figs. 1b-e), to investigate how the evolving composition and mixing of different fluids affect the boron systematics in MDACs. The simulated sediment column was assigned with different pH, $\delta^{11}B_{pw}$ as well as the concentrations of B_{pw} and DIC in the diagenetic fluids at the bottom model grid, which are the primary model inputs. Given that aragonite is the dominant carbonate phase in the studied MDAC samples, only aragonite precipitation and boron incorporation reactions are explicitly modelled by CrunchFlow (see *Supplementary material* for details). Although other biogeochemical reactions, such as AOM, that have substantial effects on MDAC formation are not simulated directly, their influence is accounted for by the different compositions of diagenetic fluid assigned. We simulated the formation of MDAC until the newly formed aragonite completely fills up the pore space, which takes a few hundred years (200-700 years) depending on the composition of the diagenetic fluid assigned. Equilibrium is never assumed in the model as we are aware that the system could be subject to disequilibrium due to the dynamic nature of cold seeps. We investigated how the boron systematics in both pore fluid and MDAC vary during the time span of MDAC formation, with the aim

of exploring the controls on their boron compositions in these dynamic settings.

CrunchFlow calculates dissolved species activities with the extended Debye-Hückel formulation which is only applicable for solution with low ionic strength (e.g., less than 0.1M). This represents an important caveat in determining the activity coefficients for aqueous species, which may be 3-15 % lower than those calculated using the Pitzer model. Nonetheless, as the processes considered in this study are dominated by kinetics rather than thermodynamics, we believe such a choice of activity coefficients will not substantially affect our model results. The minor calcite present in the MDAC samples (<14 %; Table 1) also has limited effect on the overall $\delta^{11}B_{MDAC}$ and thus our modelling results (see section 3.3 for details).

3. Results and discussion

3.1. Boron systematics in pore fluids and MDACs

We report pore fluid data from Vestnesa Ridge (Fig. 2), where four of our MDAC samples were recovered (Fig. 1a). Even though the depth scale of the profile shown in Fig. 2 (*ca*. 15 meters) is not comparable to the scale for the sediment depths where MDACs precipitate (at most a few tens of centimetres below seafloor) these pore fluid data provide a general guide for the concentrations of the relevant solutes given the dynamic nature of the seep environments. From cold seep environments, pore fluids at shallow depths often preserve source geochemical signals from greater depths (Füri et al., 2009; Scholz et al., 2010; Hong et al., 2019; Sauer et al., 2021), as the fast-ascending fluids are very resistant to diffusional mixing. Note also that the investigated MDACs formed in seep environments experiencing several fluid flow events during the past 42 to 156 kyr (Himmler et al., 2019), so while the modern fluids serve as a guide for the boron systematics in such settings, they do not necessarily reflect the fluid composition at the time of MDAC formation.

The concentrations of B_{pw} increase from 0.42 mM in the shallowest sample, which is similar to bottom seawater, to 0.56 mM in the deepest sample at *ca*. 15 mbsf. The $\delta^{11}B_{pw}$ values decrease from the seawater value of +39.6 ‰ down to +37.4 ‰ in the first meter and then gradually increase with depth to +39.5 ‰ in the deepest sample. The lower $\delta^{11}B_{pw}$ values in the top four meters of the sediments, as compared to the seawater value, may be associated with NH_4-induced boron desorption from clay surfaces (Hüpers et al. (2016) and see Hong et al. (2021) for a thorough discussion of the pore fluid data). The decrease in B_{pw}/DIC ratios from 0.09 to 0.02 mol/mol within the topmost 75 cm of sediments is due to the increase of DIC concentrations (4.6 to 25.3 mM; Fig. 2c) as the result of AOM. In deeper sediments, the ratios are relatively constant with depth with no apparent variation within the intervals where MDAC samples were recovered.

Anomalous high B_{pw} concentrations and low $\delta^{11}B_{pw}$ were observed from the two intervals (6-8 and 10-12 mbsf; Fig. 2) where gas hydrates and MDACs were recovered (Pape et al., 2020; Himmler et al., 2019). Even though gas hydrate dissociation may serve as a potential source of B_{pw} with low $\delta^{11}B_{pw}$ values as proposed previously (Kopf et al. 2000), the low B_{pw} concentrations released by gas hydrate dissociation cannot explain the elevated concentrations of B_{pw} observed in these intervals from our porewater (Hong et al., 2021), a similar conclusion made in previous studies (Teichert et al., 2005; Hüpers et al., 2016). Similarly, gas hydrate formation cannot explain the high B_{pw} concentrations detected as such a process will concentrate all solutes in the residual fluid and result in B_{pw}/Cl ratios similar to the seawater ratio (*ca*. 0.73 mmol/mol; Fig. 2e). We however observe higher B_{pw}/Cl ratios within these two intervals (Fig. 2e) that point to a dissolved boron source independent from gas hydrate dynamics. A fluid originated from greater depths carrying dissolved boron from clay desorption is the most likely explanation for the high B_{pw} concentrations and low $\delta^{11}B_{pw}$ values in the solution and may have helped determine the boron systematics in the MDACs from the same intervals. This may suggest that gas hydrate formation is associated with these instances of anomalous fluid flow, as supported by the high $\delta^{18}O$ and δD values in pore fluids (indications of active gas hydrate formation) from the same intervals (Hong et al., 2021).

The micritic cements (MCs) by nature have heterogeneous mineral composition that is represented by mixtures of aragonite and Mg-calcite (*ca*. 51 % to 94 % of bulk sample is carbonate; Table 1) along with silicate minerals that give the rise to their grey colour (Figs. 1b-c). The cavity-filling cements (CFCs), which appear white due to the higher carbonate abundance, are composed primarily of aragonite (>90 %; Table 1). The CFCs typically contain very little detrital sediment impurities, as reflected by the low aluminium concentration detected in the leachate (Table 2). The $\delta^{11}B_{MDAC}$ after the sequential leaching are in the range of +6.9 to +13.5 ‰ with B_{MDAC}/Ca ratios from 23 to 72 µmol/mol (Table 2). The slightly elevated aluminium concentrations (0.1 to 34 µM) in the leachate suggest a trace contribution of boron from the silicate minerals (<5 %; Table 2). The silicate-corrected $\delta^{11}B_{MDAC}$ values range from +7.1 to +13.5 ‰ with B_{MDAC}/Ca ratios of 22 to 72 µmol/mol (Table 2). In general, we observe similar B_{MDAC}/Ca ratios between the two types of cements but higher and more uniform $\delta^{11}B_{MDAC}$ from CFCs (+12.6 to +13.5 ‰) as compared to the MCs (+7.1 to +13.1 ‰; Table 2). We note that the sample with the lowest $\delta^{11}B_{MDAC}$ value (MC-4CC-M, +7.1 ‰) happens to have the highest aluminium content. However, this sample also has the second highest calcium content in the leachate (95 mM; Table 2). The fraction of silicate-associated boron, f_{Si}, calculated for this sample is only less than half of the highest fraction from sample MC-M13 that has a $\delta^{11}B_{MDAC}$ value of +12.3 ‰ before correction (Table 2). Since there is no apparent correlation between f_{Si} and the un-corrected $\delta^{11}B_{MDAC}$ values (Pearson correlation coefficient, R, equals −0.08 with a p value of 0.84), we interpret the low $\delta^{11}B_{MDAC}$ value from MC-4CC-M as reflecting the genuine authentic carbonate signal.

3.2. MDAC formation in fluids with low $\delta^{11}B_{pw}$ and B_{pw}/DIC values

We calculated the expected $\delta^{11}B_{arg}$ based on the range of $\delta^{11}B_{pw}$ from seawater and Vestnesa Ridge pore fluids as well as the expected pore fluid pH (7.5 to 8.4 from Reimers et al., 1996) as indicated by the blue shaded rectangle in Fig. 3. We assumed that only borate is incorporated in aragonite with α of 1.0272 (Klochko et al., 2006). Seawater pH and $\delta^{11}B_{pw}$ (+39.6 ‰) are unable to explain the observed $\delta^{11}B_{MDAC}$ values (blue cross symbol in Fig. 3). The measured $\delta^{11}B_{MDAC}$ values between +12.6 and +13.5 ‰ can be explained by the different combinations of pH and $\delta^{11}B_{pw}$ values along the red contour lines within the blue shaded rectangle (Fig. 3). To explain the $\delta^{11}B_{MDAC}$ values around +10 ‰, the solution pH has to be around 7.5 with a $\delta^{11}B_{pw}$ value close to +35 ‰. While such a specific condition is not unlikely from the seep environment, the pH is much lower than the values expected for cold seep environments, where the high carbonate alkalinity produced through Eq. (1) buffers the pore fluid (e.g., Reimers et al. (1996) and Fig. 2). Moreover, the likelihood that such a specific condition exists from two different cold seeps investigated (Alvheim channel in the central North Sea for MC-M4 and Vestnesa Ridge for MC-12R-M) is rather slim. While for the lowest $\delta^{11}B_{MDAC}$ value detected (+7.1 ‰), the $\delta^{11}B_{pw}$ must be lower than ca. +31.8 ‰ (Fig. 3). Such a $\delta^{11}B_{pw}$ value is lower than the values we observed from Vestnesa Ridge (Fig. 2) but has been documented from

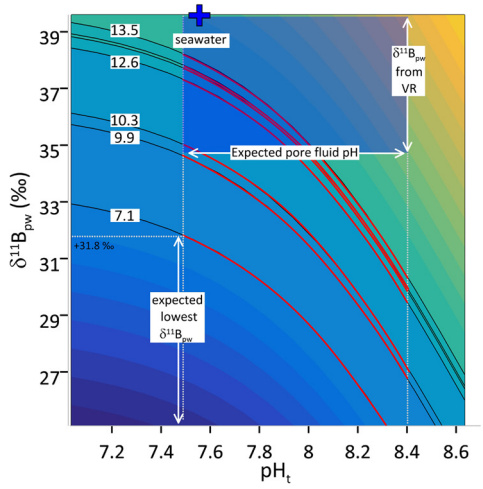

Fig. 3. Expected $\delta^{11}B_{arg}$ as a function of $\delta^{11}B_{pw}$ (data from Vestnesa Ridge, VR) and pH (in total scale, pH_t). The contours mark the values of $\delta^{11}B_{MDAC}$ in our samples (7.1-13.5 ‰; Table 2) with the red contour lines indicating the $\delta^{11}B_{MDAC}$ for the pH range expected for pore fluids (e.g., Reimers et al., 1996). The blue shaded rectangle, defined by the $\delta^{11}B_{pw}$ and pH of solution, marks the possible range of $\delta^{11}B_{arg}$ when additionally considering the observed variability in $\delta^{11}B_{pw}$ (Fig. 2). Based on these constraints, five of our MDAC samples can be explained by the expected ranges of pH and $\delta^{11}B_{pw}$ while the three samples require fluids with pH and $\delta^{11}B_{pw}$ values lower than what were observed in the modern pore fluid profile of Vestnesa Ridge.

Mediterranean mud volcanoes (Deyhle et al., 2003) and from the decollement zones (You et al., 1993).

All observed B_{MDAC}/Ca ratios from our samples are lower than the values derived from experimental precipitates (Holcomb et al., 2016) and suggest MDAC formed in DIC-rich pore fluids with B_{pw}/DIC ratios as low as *ca.* 0.020 mol/mol (Fig. S2i). Factors determining the B_{pw}/DIC ratios include the composition of fluids, which often reflects the rate of biogeochemical reactions (e.g., AOM, carbonate precipitation, and cation exchange) and the degree of mixing between seawater and the diagenetic fluids. The B_{pw}/DIC ratios from Vestnesa Ridge range from 0.017 to 0.048 mol/mol, all substantially lower than the seawater ratio of 0.205 mol/mol (Fig. 2). Though some variability in B_{pw} is expected due to boron incorporation into clays and authigenic minerals (Palmer et al., 1987; Teichert et al., 2005), the changes are not sufficiently large to explain the observed low B_{pw}/DIC ratios, which are predominantly the result of excess DIC due to intensive AOM (e.g., Sauer et al., 2021) or methanogenesis (Hong et al., 2013). For example, DIC concentrations as high as 50-80 mM have been reported reflecting the rapid carbon turnover in cold seep environments (Wallmann et al., 2008). The DIC concentrations from Vestnesa Ridge are 5 to 12 times higher than the seawater concentration (Fig. 2c). Such high DIC concentrations and the consequential low B_{pw}/DIC ratios (Fig. 2d) could explain the B_{MDAC}/Ca ratios from our samples.

3.3. Fluid composition as the primary control of $\delta^{11}B_{MDAC}$ and B_{MDAC}/Ca

Though the static view of boron equilibrium between the fluid and carbonate phases (e.g., Fig. 3) provides a useful first-order guide for the $\delta^{11}B_{arg}$ expected, it lacks the ability to consider changes of fluid composition with time and space and cannot be used to assess the effect of dynamic processes and disequilibrium on the isotopic signatures. To provide a semi-quantitative assessment of the conditions where these MDACs formed and take into account the disequilibrium between fluids and MDAC, we simulate a sediment column with different diagenetic fluid composition (Fig. 4). Such an exercise is especially critical for a highly dynamic environment, such as cold seeps, where certain diagenetic fluids - and associated precipitates - may only occur ephemerally in a confined area.

We compared the B_{arg}/Ca and $\delta^{11}B_{arg}$ values calculated by our CrunchFlow model with those reported by Holcomb et al. (2016) and Noireaux et al. (2015), respectively (Fig. S2), to calibrate the kinetic constants for aragonite precipitation/dissolution and B incorporation (see *Supplementary material* for details). Our modelled $\delta^{11}B_{arg}$ values successfully reproduced the values derived from theoretical calculation and the laboratory synthesis results (Fig. S2k). We are able to confidently model $\delta^{11}B_{arg}$ values for pH ranges between 7.5 and 8.6 with an uncertainty of around 1 ‰. Due to the issues in selecting equilibrium constants (see *Supplementary material* for more details), the model is only able to reproduce the correlation between B_{arg}/Ca and B_{pw}/DIC, but not with $B(OH)_4^-/CO_3^{2-}$ in the solution (Fig. S2i). As our measured B_{MDAC}/Ca ratios (22.0 to 71.8 µmol/mol; Table 2) are all lower than the experimentally-derived B_{arg}/Ca ratios (>100 µmol/mol from Holcomb et al. (2016); Fig. S2), our model has to extrapolate based on the trend from the literature data (e.g., data from Holcomb et al. (2016) and Fig. S2i).

To test the validity of our choice to exclude Mg-calcite, a minor carbonate component in our MDACs (Table 1), we calculated the differences in $\delta^{11}B$ between pure aragonite and MDACs (i.e. mixtures of aragonite and Mg-calcite) by considering a condition with fluid pH of 7.5 in which experimentally-grown calcite shows the greatest enrichment in ^{11}B as compared to aragonite (*ca.* 10 ‰ higher; Noireaux et al., 2015). Based on the Mg-calcite-to-aragonite ratios listed in Table 1 and assuming a binary mixing between the two types of carbonates, pure aragonite can have $\delta^{11}B$ values 0.7 to 1.6 ‰ lower than the aragonite and Mg-calcite mixtures in MDAC. In addition, calcite growth rate is also thought to be a factor influencing its $\delta^{11}B$ (Farmer et al., 2019). However, given the relatively small proportion of Mg-calcite in our samples, such fractionation (*ca.* 2 ‰ for a 10-times change in Mg-calcite precipitation rate; Farmer et al., 2019) has only a marginal effect on the overall results. Taking the sample with the highest calcite content as an example (MC-M5), the pure aragonite $\delta^{11}B$ is 1.9 ‰ lower as compared to the $\delta^{11}B$ of bulk MDAC when both the effect of pH and precipitation rate are considered (see black bars for the open symbols in Fig. 5 for all samples). Such differences, though substantial in some cases, do not significantly impact our interpretation as the variation in $\delta^{11}B_{MDAC}$, as a result of fluid composition changes, is much greater.

Our time-progressive model produces downcore pore fluid profiles (Figs. 4a, 4b, 4e) as well as the expected boron systematics of MDACs at the corresponding depths (Figs. 4c and 4f). After systematically and iteratively varying the primary model input– the fluid composition at the bottom cell– we are able to reproduce the ranges of B_{MDAC}/Ca and $\delta^{11}B_{MDAC}$ found in our studied samples (Fig. 5). For example, a scenario with a diagenetic fluid of relatively low pH (7.8) and $\delta^{11}B_{pw}$ (+32.2 ‰) values at the base of the sediment column predicts $\delta^{11}B_{MDAC}$ values as low as ca. +10 ‰ that cover most of the values measured from both CFCs and MCs, except for one sample with very low $\delta^{11}B_{MDAC}$ (+7.1 ‰; Fig. 4). The environmental inferences of such a fluid composition are further discussed in the following paragraphs when introducing model sensitivity tests (i.e. Fig. 5).

With the same lower boundary condition (i.e. constant diagenetic fluid composition), downcore mixing between seawater and the diagenetic fluids results in substantial variation in $\delta^{11}B_{arg}$ and B_{arg}/Ca values (up to 5 ‰ and >200 µmol/mol, respectively; Fig. 4). It is important to note that the amounts of boron incorporated during aragonite precipitation are very small compared to total porewater and seawater B; thus, aragonite precipitation does not affect $\delta^{11}B_{pw}$ with the rates estimated in the model. In other words, the changes in downcore pore fluid profiles reflect merely the mixing of seawater and diagenetic fluids of different composition but not boron incorporation in MDAC. From the time-variant results, it is clear that the aragonite that precipitates shallower in

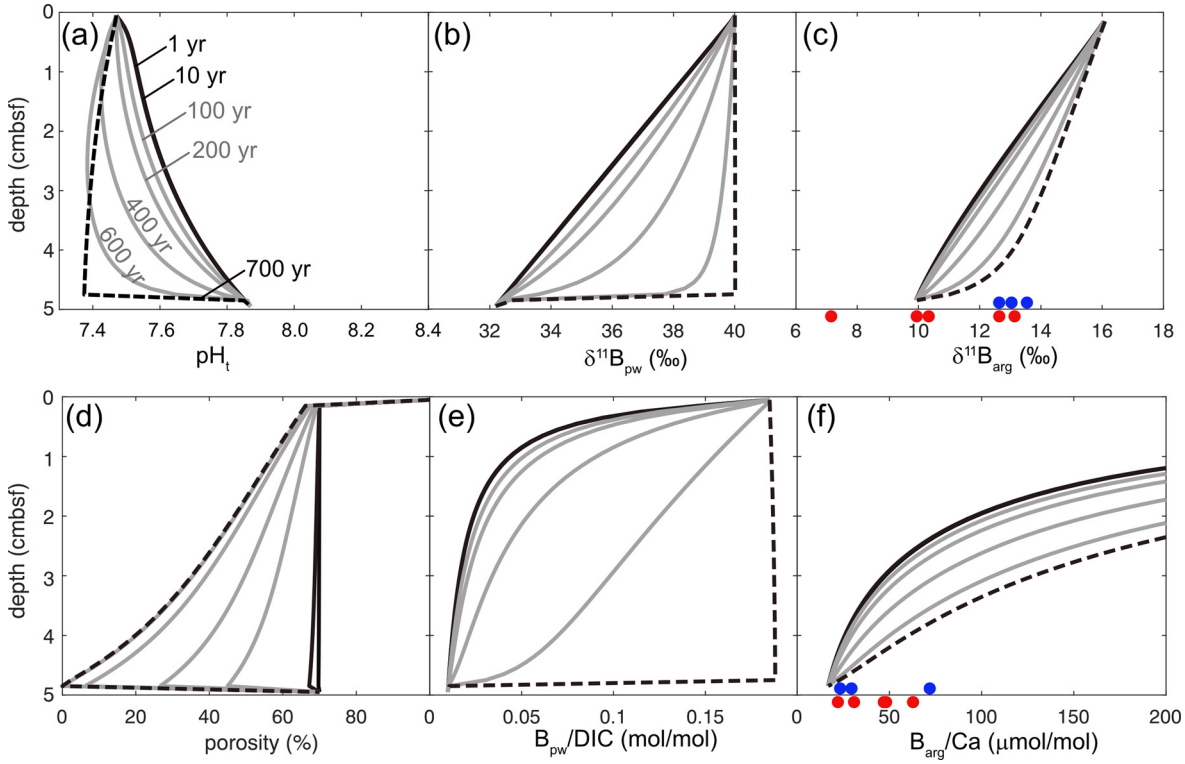

Fig. 4. Time-progressing results of a scenario from our modelling with low pH (7.8) and $\delta^{11}B_{pw}$ (+32.2 ‰) from the diagenetic fluids as the lower boundary condition (orange lines in Fig. 5). Seawater composition is assigned as the top boundary condition at zero cmbsf. Lines of different shades of grey represent snapshots of the model for specific times from 1 to 700 years. The two black solid lines, year 1 and year 10, mark the results for early periods of carbonate precipitation when only little reduction in porosity occurs. Grey lines (years 100, 200, 400 and 600) mark the transition from well-connected pores to a condition of blockage by carbonates. Large variations in both $\delta^{11}B_{arg}$ and B_{arg}/Ca can be observed during this transition phase depending on when and what sediment depth the cements form. The black dash lines (year 700) mark the final stage when the pore space is completely cemented. The range of values derived from our MDAC samples were also plotted in (c) and (f) (blue dots: CFCs; red dots: MCs). Note that the sample values do not correspond to the y-axes for depth in (c) and (f) as the exact depth of MDAC formation is unknown.

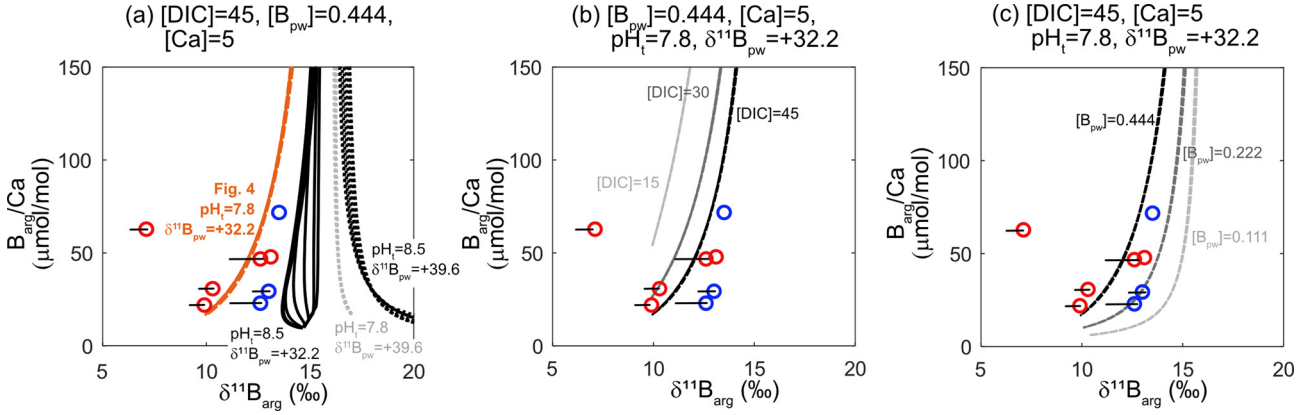

Fig. 5. Comparisons of $\delta^{11}B_{arg}$ and B_{arg}/Ca derived through modelling with different diagenetic fluid composition as indicated by the lines with different colours and patterns: (a) different $\delta^{11}B_{pw}$ and pH, (b) different DIC concentrations and (c) different porewater boron concentrations (B_{pw}). The various lines of the same pattern mark the temporal evolution in composition during the course of carbonate formation. Each of the line represents the B_{arg}/Ca-$\delta^{11}B_{arg}$ composition calculated in the model with the diagenetic fluid indicated in the headings for each plot with concentrations in millimolar and $\delta^{11}B$ in permil. Data from the three CFC samples (blue circles) and five MC samples (red circles) are shown for comparison. Error bars for each sample indicate the range of $\delta^{11}B_{MDAC}$ when calcite in the samples is considered (see section 3.3 for details). See Figs. 4 for full modelling results for the scenario in (a) (orange lines).

the sediment column could receive more seawater boron and thus display higher $\delta^{11}B_{arg}$ and B/Ca values (e.g., Figs. 4c and 4f), which may explain the higher $\delta^{11}B_{MDAC}$ values observed from CFCs, as compared to MCs. The formation of CFCs is thought to represent carbonate precipitation during periods of higher methane supplies, as compared to those for MCs. Higher methane fluxes shoal the reaction zones for carbonate precipitation and thus result in the shallower occurrence of CFCs than MCs. This is in accordance with greater influence from bottom seawater as shown by the pattern of rare earth elements in the CFCs (Himmler et al., 2010; Crémière et al., 2016b).

We present a series of model sensitivity tests in Fig. 5 to demonstrate how the changes in diagenetic fluid pH, DIC, and B_{pw} concentrations affect the boron composition in MDAC. The higher pH values in the diagenetic fluids result in $\delta^{11}B_{arg}$ values that are closer to the pore fluid and thus higher as compared to the $\delta^{11}B_{arg}$ values from low pH diagenetic fluids. For example, with a $\delta^{11}B_{pw}$ value of +32.2 ‰ assigned for the diagenetic fluid, the aragonite precipitated under a pH of 8.5 has $\delta^{11}B_{arg}$ values up to *ca.* 5 ‰

higher than those from aragonite precipitated under a pH of 7.8 (Fig. 5a, the black and orange lines, respectively). High fluid pH appears when more alkalinity is produced by faster AOM (Eq. (1)) that is sustained by a greater methane supply. Such an effect in pH may also explain the generally higher $\delta^{11}B_{MDAC}$ from the CFCs than the values from MCs, as CFCs are interpreted to precipitate under conditions of higher AOM rates (Crémière et al., 2016b). Future modelling development may include modelling the stable carbon isotopic composition (i.e. $\delta^{13}C$) of MDAC as an independent proxy of AOM.

On the other hand, variations in the DIC and B_{pw} concentrations also affect $\delta^{11}B_{arg}$ values. A higher DIC concentration in the diagenetic fluid results in aragonite with a greater downcore $\delta^{11}B_{arg}$ range (Fig. 5b). For example, when the diagenetic fluid contains 45 mM of DIC, the resulting $\delta^{11}B_{arg}$ could be between *ca.* +10 and +14.5 ‰, a range that is almost twice as large as compared to the scenario with DIC concentration of only 15 mM (between the black and light grey dash lines in Fig. 5b). This is partially due to the associated variation in carbonate precipitation rates stimulated by the different DIC concentrations in the diagenetic fluids (see section 3.4 for more details). Inversely, a lower B_{pw} value in the diagenetic fluids results in a greater range of $\delta^{11}B_{arg}$ as compared to the case with a higher B_{pw} (black and light grey dash lines in Fig. 5c). The low B_{pw} concentration in the diagenetic fluids enhances the diffusive flux of seawater boron due to a greater concentration gradient between seawater and the diagenetic fluid. Increases of $\delta^{11}B_{MDAC}$ are thus expected as more seawater-derived boron with a higher $\delta^{11}B_{pw}$ signature is incorporated into the carbonates. Despite the low B_{pw} concentrations assigned in the model (e.g., Fig. 5c), which is not necessary the case for the diagenetic fluids, the simulation highlights the effect of fluctuations in B_{pw} concentrations on $\delta^{11}B_{arg}$. The B_{MDAC}/Ca ratios are sensitive to the downcore mixing of different fluids (i.e. Fig. 4f) but not very sensitive to the composition of diagenetic fluids we assigned at the bottom cell (Fig. 5), as our observed B_{MDAC}/Ca ratios can be explained by the wide concentration ranges of DIC and B_{pw} assigned (between lines of different colours and patterns in Figs. 5b and 5c).

3.4. Changes in boron incorporation as a result of carbonate precipitation: the effect of physical properties, pH, and mineral surface kinetics

Besides fluid composition, the physical properties of sediment are also modified when MDACs precipitate in sediment pore space. The precipitation of carbonate decreases porosity (Fig. 4d) and thus dampens the mixing of fluids through diffusion. High porosity ensures efficient boron diffusion and mixing between diagenetic fluids and seawater, which is reflected by the B_{MDAC}/Ca and $\delta^{11}B_{MDAC}$ (solid black lines in Fig. 4). Ion diffusion from the diagenetic fluids becomes sluggish under the moderate blockage condition due to carbonate formation in the pore space (grey lines in Fig. 4). At a stage when the pore space is completely blocked by MDACs (dashed lines in Fig. 4), the fluids in most of the pores above the blockage are gradually replaced by seawater as the connection to the bottom diagenetic fluid below diminishes. As a result, $\delta^{11}B_{arg}$ and the B_{arg}/Ca ratios gradually increase with time (see the progressive changes in Figs. 4c & 4f) as porosity and the influence of diagenetic fluids decrease (Fig. 4d). Such an effect of porosity can also be demonstrated by varying DIC concentrations in the diagenetic fluid of our model (Fig. 5b). A lower DIC concentration in the diagenetic fluid results in a slower closure of connection between seawater and the diagenetic fluids at depth (see the lines of different colours and patterns in Fig. 5b). More isotopically light boron from the diagenetic fluid with higher B_{pw}/DIC ratios (as compared to the scenario with lower B_{pw}/DIC ratios) can therefore be incorporated before the pore space is completely clogged by carbonates. Such modelling results suggest that changes in porosity as a result of carbonate precipitation can be important when interpreting MDAC boron signals. In addition, the changes in $\delta^{11}B_{arg}$ and B_{arg}/Ca ratios with time revealed by our modelling also illustrate that steady state and equilibrium conditions cannot necessarily be assumed (e.g., Fig. 3) in these dynamic cold seep environments.

Carbonate precipitation also serves as an additional source of protons that acidifies the pore fluid (Eq. (2)). We propose that, in addition to the ^{11}B-depleted diagenetic fluids sourced from greater depths, changes of pH in the micro-environments as a result of AOM and carbonate precipitation may also influence the $\delta^{11}B_{MDAC}$ observed, in part also through the exchange of boron across the fluid-clay interface. Under an alkaline condition, such as when the pore fluid is buffered by the bicarbonate produced through AOM (Eq. (1)), borate may be adsorbed to clay/organic matter, which is depleted in ^{11}B compared to the total solution (Palmer et al., 1987; Lemarchand et al., 2005). The early stage conditions in our modelling represent such a situation with pore fluid pH reflecting mixing between diagenetic fluids and seawater with limited influence from carbonate precipitation (black solid lines in Fig. 4a). The pore fluid at this stage is more basic as compared to the fluids in the later stages that are heavily modified by carbonate precipitation (e.g., grey and black dash lines in Fig. 4). When the solution becomes more acidic, as a result of carbonate precipitation (Eq. (2)), the release of ^{11}B-depleted boron to solution will occur. The incorporation of such boron may explain the low $\delta^{11}B_{MDAC}$ of our samples (including both MCs and CFCs) compared to carbonates formed in seawater (Fig. 3). Though not currently accounted for in our numerical model, such a release of low $\delta^{11}B$ could occur during the transition stage as characterized by dramatic lowering in pore fluid pH (grey lines in Fig. 4a). To a first-order, the effect of exchangeable boron release from clay surfaces can be demonstrated by considering the experiments from Palmer et al. (1987) who find considerable uptake of boron onto clay surfaces (i.e. $K_D = 2.6 g/g$ at pH 7.8) with α of 1.0253. Assuming the initial solution has a $\delta^{11}B_{pw}$ of +39.6 ‰ (i.e. seawater B), the $\delta^{11}B$ for the adsorbed boron and final solution will be +32.2 ‰ and +58.5 ‰, respectively. If the adsorbed boron is released back to the solution during carbonate precipitation, the modelled aragonite forming at pH values between 7.8 and 8.5 would have $\delta^{11}B_{arg}$ values that match with many of the $\delta^{11}B_{MDAC}$ values from our samples (orange dash and black solid lines in Fig. 5a). Clay surface kinetics may thus exert a potentially important influence on boron concentration and isotopic composition in these settings. Our first-order calculation above serves to illustrate that incorporation of exchangeable boron into MDACs may be an important aspect of interpreting the signals in these settings, and highlights the necessity to include clay surface kinetics in future assessments.

4. Conclusions

Through a newly developed sequential leaching protocol, we isolate boron signals from MDACs to constrain the fluid condition during carbonate precipitation in three cold seeps along the Norwegian margin. We observe lower $\delta^{11}B_{MDAC}$ values and B_{MDAC}/Ca ratios from studied MDACs as compared to the carbonates in equilibrium with seawater. With assistance from a numerical model calibrated with empirical data, we identify factors that contribute to the anomalous boron signatures observed from our MDACs. We show that the changes in pore fluid composition due to the different degrees of mixing between seawater and the diagenetic fluids, as well as changing biogeochemical reaction rates, all contribute to these observations. The low $\delta^{11}B_{MDAC}$ values are attributed to the low $\delta^{11}B_{pw}$ values that either hint at high-temperature modification of fluids at great depths or the incorporation of exchangeable boron under fluctuating pH due to intensive AOM and carbonate

precipitation. Faster turnover of methane through AOM also increases DIC concentrations and thus results in abrupt decreases in the B_{pw}/DIC ratios across the diagenetic zone and explains the low B_{MDAC}/Ca ratios observed. The generally higher $\delta^{11}B_{MDAC}$ from the cavity-filling cements, as compared to the micritic cements, can be explained by conditions associated with faster AOM and shallower sediment depths of formation for cavity-filling cements. The intensive carbonate precipitation under such a high methane flux can rapidly terminate the connection to the diagenetic fluid supply by reducing porosity, which decreases the relative fluid contribution from the diagenetic fluid and results in higher $^{11}B_{MDAC}$ values in the carbonate that forms after the pore space closure. Our study demonstrates the uncertainties when making inferences about paleo-fluid conditions from carbonate $\delta^{11}B$ and B/Ca values. The feedback among the different factors (e.g., fluid composition, depth of formation, physical properties, mineral surface kinetics) complicates a straightforward interpretation (e.g., Fig. 3). Nonetheless, numerical models that consider laboratory experiment results and first principles have the potential to constrain the range of past conditions that best explain the observed boron systematics from geological carbonate archives.

CRediT authorship contribution statement

Wei-Li Hong: Conceptualization, Formal analysis, Methodology, Software, Validation, Visualization, Writing – original draft. **Aivo Lepland:** Conceptualization, Funding acquisition, Project administration, Resources, Validation, Writing – review & editing. **Kalle Kirsimäe:** Investigation, Writing – review & editing. **Antoine Crémière:** Writing – review & editing. **James W.B. Rae:** Conceptualization, Methodology, Validation, Writing – review & editing.

Declaration of competing interest

The authors declare that they have no known competing financial interests or personal relationships that could have appeared to influence the work reported in this paper.

Acknowledgements

The work is supported by Norwegian Research Council through the schemes PETROMAKS2-NORCRUST (grant number 255150) and Centre for Arctic Gas Hydrate, Environment and Climate (CAGE grant number 223259) as well as Lundin Norway AS. We acknowledge the crews and captain from R/V 'MARIA S. MERIAN' as well as the MeBo team and the cruise participants during cruise MSM57-1/-2. Cruise MSM57-1/-2 was funded by the German Research Foundation (DFG), the Research Center/Excellence Cluster "The Ocean in the Earth System" at MARUM–Center for Marine and Environmental Sciences, University of Bremen and funds from CAGE. We would also like to acknowledge two anonymous reviewers for their insightful and constructive comments that significantly improve the quality of this paper.

Appendix A. Supplementary material

Supplementary material related to this article can be found online at https://doi.org/10.1016/j.epsl.2021.117337.

References

Bellefroid, E.J., Planavsky, N.J., Miller, N.R., Brand, U., Wang, C., 2018. Case studies on the utility of sequential carbonate leaching for radiogenic strontium isotope analysis. Chem. Geol. 497, 88–99.

Boetius, A., Ravenschlag, K., Schubert, C.J., Rickert, D., Widdel, F., Gleseke, A., Amann, R., Jørgensen, B.B., Witte, U., Pfannkuche, O., 2000. A marine microbial consortium apparently mediating anaerobic oxidation methane. Nature 407, 623–626. Available at: www.nature.com. (Accessed 19 October 2020).

Bohrmann, G., Ahrlich, F., Bergenthal, M., Bünz, S., Düßmann, R., Ferreira, C., Freudenthal, T., Fröhlich, S., Hamann, K., Hong, W.-L., Hsu, Ch.-W., 2017. R/V MARIA S. MERIAN Cruise Report MSM57, Gas Hydrate Dynamics at the Continental Margin of Svalbard Reykjavik–Longyearbyen–Reykjavik, 29 July–07 September 2016. Available at: www.geo.uni-bremen.de. (Accessed 19 October 2020).

Crémière, A., Lepland, A., Chand, S., Sahy, D., Condon, D.J., Noble, S.R., Martma, T., Thorsnes, T., Sauer, S., Brunstad, H., 2016a. Timescales of methane seepage on the Norwegian margin following collapse of the Scandinavian Ice Sheet. Nat. Commun. 7, 1–10. Available at: www.nature.com/naturecommunications. (Accessed 20 October 2020).

Crémière, A., Lepland, A., Chand, S., Sahy, D., Kirsimäe, K., Bau, M., Whitehouse, M.J., Noble, S.R., Martma, T., Thorsnes, T., Brunstad, H., 2016b. Fluid source and methane-related diagenetic processes recorded in cold seep carbonates from the Alvheim channel, central North Sea. Chem. Geol. 432, 16–33.

DeCarlo, T.M., Holcomb, M., McCulloch, M.T., 2018. Reviews and syntheses: revisiting the boron systematics of aragonite and their application to coral calcification. Biogeosciences 15, 2819–2834.

Deyhle, A., Kopf, A., 2001. Deep fluids and ancient pore waters at the backstop: stable isotope systematics (B, C, O) of mud-volcano deposits on the Mediterranean Ridge accretionary wedge. Geology 29, 1031. Available at: https://pubs.geoscienceworld.org/geology/article/29/11/1031-1034/197873. (Accessed 18 May 2020).

Deyhle, A., Kopf, A.J., Aloisi, G., 2003. Boron and boron isotopes as tracers for diagenetic reactions and depth of mobilization, using muds and authigenic carbonates from eastern Mediterranean mud volcanoes. Geol. Soc. Spec. Publ. 216, 491–503. Available at: http://sp.lyellcollection.org/. (Accessed 26 January 2021).

Dickson, A.G., 1990. Thermodynamics of the dissociation of boric acid in synthetic seawater from 273.15 to 318.15 K. Deep-Sea Res., A, Oceanogr. Res. Pap. 37, 755–766.

Farmer, J.R., Branson, O., Uchikawa, J., Penman, D.E., Hönisch, B., Zeebe, R.E., 2019. Boric acid and borate incorporation in inorganic calcite inferred from B/Ca, boron isotopes and surface kinetic modeling. Geochim. Cosmochim. Acta 244, 229–247.

Foster, G.L., 2008. Seawater pH, pCO2 and [CO2−3] variations in the Caribbean Sea over the last 130 kyr: a boron isotope and B/Ca study of planktic foraminifera. Earth Planet. Sci. Lett. 271, 254–266. Available at: https://linkinghub.elsevier.com/retrieve/pii/S0012821X08002549. (Accessed 18 May 2020).

Foster, G.L., Hönisch, B., Paris, G., Dwyer, G.S., Rae, J.W.B., Elliott, T., Gaillardet, J.Ô., Hemming, N.G., Louvat, P., Vengosh, A., 2013. Interlaboratory comparison of boron isotope analyses of boric acid, seawater and marine CaCO3 by MC-ICPMS and NTIMS. Chem. Geol. 358, 1–14.

Foster, G.L., Pogge von Strandmann, P.A.E., Rae, J.W.B., 2010. Boron and magnesium isotopic composition of seawater. Geochem. Geophys. Geosyst. 11.

Freudenthal, T., Wefer, G., 2013. Drilling cores on the sea floor with the remote-controlled sea floor drilling rig MeBo. Geosci. Instrum. Method. Data Syst. 2, 329–337.

Füri, E., Hilton, D.R., Brown, K.M., Tryon, M.D., 2009. Helium systematics of cold seep fluids at Monterey Bay, California, USA, temporal variations and mantle contributions. Geochem. Geophys. Geosyst. 10 (8).

Gagnon, A.C., Gothmann, A.M., Branson, O., Rae, J.W.B., Stewart, J.A., 2021. Controls on boron isotopes in a cold-water coral and the cost of resilience to ocean acidification. Earth Planet. Sci. Lett. 554, 116662.

Hemming, N.G., Hanson, G.N., 1992. Boron isotopic composition and concentration in modern marine carbonates. Geochim. Cosmochim. Acta 56, 537–543.

Hemming, N.G., Reeder, R.J., Hanson, G.N., 1995. Mineral-fluid partitioning and isotopic fractionation of boron in synthetic calcium carbonate. Geochim. Cosmochim. Acta 59, 371–379.

Himmler, T., Bach, W., Bohrmann, G., Peckmann, J., 2010. Rare Earth elements in authigenic methane-seep carbonates as tracers for fluid composition during early diagenesis. Chem. Geol. 277, 126–136.

Himmler, T., Sahy, D., Martma, T., Bohrmann, G., Plaza-Faverola, A., Bünz, S., Condon, D.J., Knies, J., Lepland, A., 2019. A 160,000-year-old history of tectonically controlled methane seepage in the Arctic. Sci. Adv. 5, eaaw1450. Available at: http://advances.sciencemag.org/. (Accessed 20 October 2020).

Holcomb, M., DeCarlo, T.M., Gaetani, G.A., McCulloch, M., 2016. Factors affecting B/Ca ratios in synthetic aragonite. Chem. Geol. 437, 67–76.

Hong, W-L., Pape, Thomas, Schmidt, Christopher, Yao, Haoyi, Wallmann, K., Plaza-Faverola, Andreia, Rae, J.W.B., Lepland, Aivo, Bünz, Stefan, Bohrmann, Gerhard, 2021. Interactions between deep formation fluid and gas hydrate dynamics inferred from pore fluid geochemistry at active pockmarks of the Vestnesa Ridge, west Svalbard margin. Mar. Pet. Geol. 127, 104957.

Hong, W.L., Latour, P., Sauer, S., Sen, A., Gilhooly, W.P., Lepland, A., Fouskas, F., 2020. Iron cycling in Arctic methane seeps. Geo Mar. Lett. 40, 391–401. https://doi.org/10.1007/s00367-020-00649-5. [Accessed October 20, 2020].

Hong, W.L., Lepland, A., Himmler, T., Kim, J.H., Chand, S., Sahy, D., Solomon, E.A., Rae, J.W., Martma, T., Nam, S.I., Knies, J., 2019. Discharge of meteoric water in the eastern Norwegian Sea since the last glacial period. Geophys. Res. Lett. 46 (14), 8194–8204.

Hong, W.-L., Torres, M.E., Kim, J.-H., Choi, J., Bahk, J.-J., 2013. Carbon cycling within the sulfate-methane-transition-zone in marine sediments from the Ulleung basin. Biogeochemistry 115, 129–148.

Hönisch, B., Eggins, S.M., Haynes, L.L., Allen, K.A., Holland, K.D., Lorbacher, K., 2019. Boron Proxies in Paleoceanography and Paleoclimatology. John Wiley & Sons, Ltd, Chichester, UK. Available at: http://doi.wiley.com/10.1002/9781119010678. (Accessed 25 January 2021).

Hüpers, A., Kasemann, S.A., Kopf, A.J., Meixner, A., Toki, T., Shinjo, R., Wheat, C.G., You, C.F., 2016. Fluid flow and water–rock interaction across the active Nankai Trough subduction zone forearc revealed by boron isotope geochemistry. Geochim. Cosmochim. Acta 193, 100–118.

Kiss, E., 1988. Ion-exchange separation and spectrophotometric determination of boron in geological materials. Anal. Chim. Acta 211, 243–256.

Klochko, K., Kaufman, A.J., Yao, W., Byrne, R.H., Tossell, J.A., 2006. Experimental measurement of boron isotope fractionation in seawater. Earth Planet. Sci. Lett. 248, 276–285.

Lemarchand, E., Schott, J., Gaillardet, J., 2005. Boron isotopic fractionation related to boron sorption on humic acid and the structure of surface complexes formed. Geochim. Cosmochim. Acta 69, 3519–3533.

Loyd, S.J., Sample, J., Tripati, R.E., Defliese, W.F., Brooks, K., Hovland, M., Torres, M., Marlow, J., Hancock, L.G., Martin, R., Lyons, T., Tripati, A.E., 2016. Methane seep carbonates yield clumped isotope signatures out of equilibrium with formation temperatures. Nat. Commun. 7, 1–12. Available at: www.nature.com/naturecommunications. (Accessed 19 October 2020).

Luff, R., Wallmann, K., 2003. Fluid flow, methane fluxes, carbonate precipitation and biogeochemical turnover in gas hydrate-bearing sediments at hydrate ridge, Cascadia margin: numerical modeling and mass balances. Geochim. Cosmochim. Acta 67, 3403–3421.

Mavromatis, V., Montouillout, V., Noireaux, J., Gaillardet, J., Schott, J., 2015. Characterization of boron incorporation and speciation in calcite and aragonite from co-precipitation experiments under controlled pH, temperature and precipitation rate. Geochim. Cosmochim. Acta 150, 299–313.

Noireaux, J., Mavromatis, V., Gaillardet, J., Schott, J., Montouillout, V., Louvat, P., Rollion-Bard, C., Neuville, D.R., 2015. Crystallographic control on the boron isotope paleo-pH proxy. Earth Planet. Sci. Lett. 430, 398–407.

Palmer, M.R., Spivack, A.J., Edmond, J.M., 1987. Temperature and pH controls over isotopic fractionation during adsorption of boron on marine clay. Geochim. Cosmochim. Acta 51, 2319–2323.

Pape, T., Bünz, S., Hong, W.L., Torres, M.E., Riedel, M., Panieri, G., Lepland, A., Hsu, C.W., Wintersteller, P., Wallmann, K., Schmidt, C., Yao, H., Bohrmann, G., 2020. Origin and transformation of light hydrocarbons ascending at an active pockmark on vestnesa ridge, Arctic Ocean. J. Geophys. Res., Solid Earth 125. Available at: https://agupubs.onlinelibrary.wiley.com/doi/full/10.1029/2018JB016679. (Accessed 19 October 2020).

Paris, G., Bartolini, A., Donnadieu, Y., Beaumont, V., Gaillardet, J., 2010. Investigating boron isotopes in a middle Jurassic micritic sequence: primary vs. diagenetic signal. Chem. Geol. 275, 117–126.

Peckmann, J., Reimer, A., Luth, U., Luth, C., Hansen, B.T., Heinicke, C., Hoefs, J., Reitner, J., 2001. Methane-derived carbonates and authigenic pyrite from the northwestern Black Sea. Mar. Geol. 177, 129–150.

Rae, J.W.B., Burke, A., Robinson, L.F., Adkins, J.F., Chen, T., Cole, C., Greenop, R., Li, T., Littley, E.F.M., Nita, D.C., Stewart, J.A., Taylor, B.J., 2018. CO2 storage and release in the deep Southern Ocean on millennial to centennial timescales. Nature 562, 569–573.

Rae, J.W.B., Foster, G.L., Schmidt, D.N., Elliott, T., 2011. Boron isotopes and B/Ca in benthic foraminifera: proxies for the deep ocean carbonate system. Earth Planet. Sci. Lett. 302, 403–413.

Reeburgh, W.S., 2007. Oceanic methane biogeochemistry. Chem. Rev. 107, 486–513. Available at: https://pubs.acs.org/sharingguidelines. (Accessed 19 October 2020).

Reimers, C.E., Ruttenberg, K.C., Canfield, D.E., Christiansen, M.B., Martin, J.B., 1996. Porewater pH and authigenic phases formed in the uppermost sediments of the Santa Barbara basin. Geochim. Cosmochim. Acta 60, 4037–4057.

Sauer, S., Hong, W.L., Yao, H., Lepland, A., Klug, M., Eichinger, F., Himmler, T., Crémière, A., Panieri, G., Schubert, C.J., Knies, J., 2021. Methane transport and sources in an Arctic deep-water cold seep offshore NW Svalbard (Vestnesa Ridge, 79° N). Deep-Sea Res., Part 1, Oceanogr. Res. Pap. 167, 103430.

Schier, K., Himmler, T., Lepland, A., Kraemer, D., Schönenberger, J., Bau, M., 2021. Insights into the REY inventory of seep carbonates from the Northern Norwegian margin using geochemical screening. Chem. Geol. 559, 119857.

Scholz, F., Hensen, C., De Lange, G.J., Haeckel, M., Liebetrau, V., Meixner, A., Reitz, A., Romer, R.L., 2010. Lithium isotope geochemistry of marine pore waters–insights from cold seep fluids. Geochim. Cosmochim. Acta 74 (12), 3459–3475.

Shao, J., Stott, L.D., Gray, W.R., Greenop, R., Pecher, I., Neil, H.L., Coffin, R.B., Davy, B., Rae, J.W.B., 2019. Atmosphere-ocean CO2 exchange across the last deglaciation from the boron isotope proxy. Paleoceanogr. Paleoclimatol. 34, 1650–1670. Available at: https://agupubs.onlinelibrary.wiley.com/doi/full/10.1029/2018PA003498. (Accessed 3 February 2021).

Steefel, C.I., Appelo, C.A.J., Arora, B., Jacques, D., Kalbacher, T., Kolditz, O., Lagneau, V., Lichtner, P.C., Mayer, K.U., Meeussen, J.C.L., Molins, S., Moulton, D., Shao, H., Šimůnek, J., Spycher, N., Yabusaki, S.B., Yeh, G.T., 2015. Reactive transport codes for subsurface environmental simulation. Comput. Geosci. 19, 445–478. Available at: https://link.springer.com/article/10.1007/s10596-014-9443-x. (Accessed 19 October 2020).

Suess, E., 2014. Marine cold seeps and their manifestations: geological control, biogeochemical criteria and environmental conditions. Int. J. Earth Sci. 103, 1889–1916. Available at: https://link.springer.com/article/10.1007/s00531-014-1010-0. (Accessed 19 October 2020).

Teichert, B.M.A., Torres, M.E., Bohrmann, G., Eisenhauer, A., 2005. Fluid sources, fluid pathways and diagenetic reactions across an accretionary prism revealed by Sr and B geochemistry. Earth Planet. Sci. Lett. 239, 106–121.

Thiagarajan, N., Crémière, A., Blättler, C., Lepland, A., Kirsimäe, K., Higgins, J., Brunstad, H., Eiler, J., 2020. Stable and clumped isotope characterization of authigenic carbonates in methane cold seep environments. Geochim. Cosmochim. Acta 279, 204–219.

Uchikawa, J., Penman, D.E., Zachos, J.C., Zeebe, R.E., 2015. Experimental evidence for kinetic effects on B/Ca in synthetic calcite: implications for potential B(OH)4- and B(OH)3 incorporation. Geochim. Cosmochim. Acta 150, 171–191.

Vengosh, A., Kolodny, Y., Starinsky, A., Chivas, A.R., McCulloch, M.T., 1991. Coprecipitation and isotopic fractionation of boron in modern biogenic carbonates. Geochim. Cosmochim. Acta 55, 2901–2910.

Wallmann, K., Aloisi, G., Haeckel, M., Tishchenko, P., Pavlova, G., Greinert, J., Kutterolf, S., Eisenhauer, A., 2008. Silicate weathering in anoxic marine sediments. Geochim. Cosmochim. Acta 72, 2895–2918.

You, C.-F., Spivack, A.J., Smith, J.H., Gieskes, J.M., 1993. Mobilization of boron in convergent margins: implications for the boron geochemical cycle. Geology 21, 207–210.

Zeebe, R.E., Rae, J.W.B., 2020. Equilibria, kinetics, and boron isotope partitioning in the aqueous boric acid–hydrofluoric acid system. Chem. Geol. 550, 119693.